Nuclear spin dependence of the reaction of H_3^+ with H_2. II. Experimental measurements

Kyle N. Crabtree,[1] Carrie A. Kauffman,[1] Brian A. Tom,[1,a)] Eftalda Beçka,[1]
Brett A. McGuire,[1,b)] and Benjamin J. McCall[2,c)]
[1]*Department of Chemistry, University of Illinois, Urbana, Illinois 61801, USA*
[2]*Departments of Chemistry, Astronomy, and Physics, University of Illinois, Urbana, Illinois 61801, USA*

(Received 26 January 2011; accepted 17 April 2011; published online 19 May 2011)

The nuclear spin dependence of the chemical reaction $H_3^+ + H_2 \rightarrow H_2 + H_3^+$ has been studied in a hollow cathode plasma cell. Multipass infrared direct absorption spectroscopy has been employed to monitor the populations of several low-energy rotational levels of *ortho*- and *para*-H_3^+ (*o*-H_3^+ and *p*-H_3^+) in hydrogenic plasmas of varying *para*-H_2 (*p*-H_2) enrichment. The ratio of the rates of the proton hop (k^H) and hydrogen exchange (k^E) reactions $\alpha \equiv k^H/k^E$ is inferred from the observed *p*-H_3^+ fraction as a function of *p*-H_2 fraction using steady-state chemical models. Measurements have been performed both in uncooled ($T_{kin} \sim 350$ K) and in liquid-nitrogen-cooled ($T_{kin} \sim 135$ K) plasmas, marking the first time this reaction has been studied at low temperature. The value of α has been found to decrease from 1.6 ± 0.1 at 350 K to 0.5 ± 0.1 at 135 K. © *2011 American Institute of Physics*. [doi:10.1063/1.3587246]

I. INTRODUCTION

The most abundant element in the universe is hydrogen, and consequently it can be argued that the chemistry and physics of hydrogenic species are the most important on a universal scale. Moreover, as the simplest of the elements, hydrogen has often been used as the benchmark species for testing computational techniques in quantum mechanics. Even with the impressive body of work accumulated about hydrogen, some areas are still undergoing active study.

One such area is the chemical physics of ion-molecule reactions. Hydrogenic ion-molecule reactions are excellent candidates for comparison of theoretical methods with experimental results. The simplest of these, the reaction of H^+ with H_2, has been extensively studied (see Jambrina *et al.*[1] and references therein), as has the simplest bimolecular reaction, $H_2^+ + H_2$.[2,3] In each of these cases, fully quantum reactive scattering calculations are still quite challenging, but statistical models and/or semiclassical calculations have been shown to agree reasonably well with experimental measurements.

The next member in this series is the simplest bimolecular reaction involving a polyatomic, $H_3^+ + H_2$. H_3^+ has long been known to be an important player in interstellar chemistry, helping to initiate the ion-molecule reactions responsible for forming polyatomic molecules in space,[4,5] and is also a useful probe of astrophysical conditions.[6–8] The $H_3^+ + H_2$ reaction has important implications for its use as an interstellar temperature probe,[9] and its deuterated variants are among the most important reactions involved in deuterium fractionation in the interstellar medium.[10]

While the deuterated forms of the $H_3^+ + H_2$ reaction have been studied extensively in the laboratory,[11–14] the purely hydrogenic system has not been as well-studied experimentally. When H_3^+ reacts with H_2, there are three possible outcomes:

$$\tilde{H}_3^+ + H_2 \rightarrow \tilde{H}_3^+ + H_2, \tag{1}$$

$$\tilde{H}_3^+ + H_2 \rightarrow H_2\tilde{H}^+ + \tilde{H}_2, \tag{2}$$

$$\tilde{H}_3^+ + H_2 \rightarrow H\tilde{H}_2^+ + H\tilde{H}. \tag{3}$$

These are defined as the identity (1), proton hop (2), and hydrogen exchange (3) processes, with statistical weights 1, 3, and 6, respectively. Each is subject to nuclear spin selection rules,[15,16] and consequently the ratio of their rates ($\alpha \equiv k^H/k^E$, where k^H and k^E are the hop and exchange rate coefficients, respectively) can be inferred by observing the *ortho*:*para* ratio of H_3^+ in hydrogenic plasmas of varying *ortho*:*para* H_2 ratio (more details will be given in Sec. IV). The lone experimental study of this reaction found $\alpha = 2.4 \pm 0.6$ in a ~400 K hollow cathode plasma,[17] well above the statistical limit of $\alpha = 3/6 = 0.5$. This is roughly consistent with a study of the $D_3^+ + H_2$ system,[11] which found that α increased well above its statistical limit with increasing collision energy.

As a consequence of the dearth of experimental data available for this reaction, theoretical efforts have been limited. Full dimensional potential energy surfaces for H_5^+ are available,[18,19] but no quasiclassical trajectory calculations have been published to our knowledge. The only efforts at calculating rate coefficients for these processes have been microcanonical statistical calculations.[14,20] Experimental measurements of the $H_3^+ + H_2$ system, especially at low temperature, are necessary for validating these models and providing data against which future theoretical calculations can be judged.

a)Present address: Department of Chemistry, United States Air Force Academy, CO 80840, USA.
b)Present address: Department of Chemistry, Emory University, Atlanta, GA 30322, USA.
c)Electronic mail: bjmccall@illinois.edu.

TABLE I. The rotational levels used in this work and their target transitions. Energies are relative to the forbidden $(J, K) = (0, 0)$ level. Energies and transition frequencies are taken from literature values (Ref. 22). Transition dipole moments are calculated from the Einstein A coefficients (Ref. 23).

Rotational Level (J,K)	Type	Energy (cm^{-1})	Transition	Frequency (cm^{-1})	$\lvert\mu\rvert^2$ (D^2)
(1,1)	*para*	64.121	$R(1,1)^u$	2726.219	0.0158
(1,0)	*ortho*	86.960	$R(1,0)$	2725.898	0.0259
(2,2)	*para*	169.295	$R(2,2)^l$	2762.070	0.0177
(2,1)	*para*	237.356	$R(2,1)^u$	2826.117	0.0182
(3,3)	*ortho*	315.342	$R(3,3)^l$	2829.922	0.0191
(3,2)	*para*	428.009	$R(3,2)^u$	2923.344	0.0143
(3,1)	*para*	494.753	$R(3,1)^u$	2928.317	0.0180
(3,0)	*ortho*	516.867	$R(3,0)$	2930.145	0.0191

The structure of this paper is as follows. Section II describes the experimental approach for our study of this reaction. Section III presents the experimental results. The data are analyzed and discussed within the context of the modeling work presented in the previous article in this issue[21] in Sec. IV, and conclusions/perspectives summarized in Sec. V. Finally, throughout this paper o-H_2, p-H_2, o-H_3^+, and p-H_3^+ will be used to refer to *ortho*- and *para*-H_2 and H_3^+.

II. EXPERIMENTAL DETAILS

The objective of this experiment is to spectroscopically measure transitions arising from several of the lowest-energy rotational levels of H_3^+ in a plasma of a known *ortho*:*para* H_2 ratio. Doing so allows determination of the *ortho*:*para* H_3^+ ratio, the plasma kinetic temperature, and the H_3^+ rotational temperature. The target transitions are within the H_3^+ ν_2 fundamental band, and are listed in Table I. This experiment has three main components: a p-H_2 production system, a hollow cathode plasma cell, and a mid-infrared spectrometer.

A. p-H_2 production

Normal hydrogen gas (n-H_2, 25% p-H_2) is produced at a purity of 99.99999% by a hydrogen generator (Parker Balsten H2-1200). To produce > 99.9% p-H_2, the n-H_2 from the generator is passed over an Fe_2O_3 catalyst held at 15 K. Full details about this p-H_2 converter are given elsewhere.[24] Mixtures of 40%, 50%, 66%, and 83% p-H_2 are obtained by combining appropriate partial pressures of p-H_2 and n-H_2 in a 1 gallon cylinder, which is lined with Teflon to minimize back-conversion of p-H_2 to o-H_2. The uncertainties on the p-H_2 fractions for these mixtures are 1.0%, 1.1%, 1.2%, and 1.4%, respectively.

B. Hollow cathode cell

A hollow cathode cell based on the design of Amano[25] was used to produce pulsed hydrogenic plasmas and is illustrated in Fig. 1. The cathode consists of a 1.4 m long, 1.5 in. diameter cylindrical copper tube wrapped in 1/4 in. diameter copper tubing used for cooling the cathode, all encased in a 4 in. diameter glass tube. The water-cooled anode is situated in an extended glass tube above a 1 in. diameter hole located at the midpoint of the cathode. A pulsed electrical discharge is generated by applying a 200 μs, 1 kV pulse to the anode at ~1 Hz while grounding the cathode. The current during the pulse is uniformly 1.25 A in nearly all cases, though subtle differences are observed under different cell temperature and pressure conditions (Fig. 2).

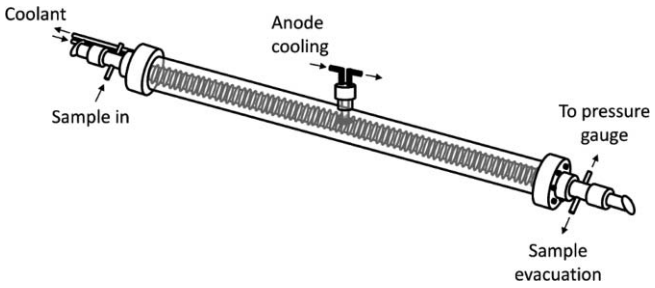

FIG. 1. Schematic drawing of the hollow cathode cell used in this study. Technical drawings are available in the supplementary material (Ref. 26).

At each end of the glass tube are stainless steel flanges with 1 in. apertures cut into the centers, sealed to the cell with silicone o-rings. Into these apertures, a glass section with tubing for sample introduction/evacuation is placed. The ends of these tubes are connected with Ultra-Torr fittings to metal pieces cut at Brewster's angle, and BaF_2 windows are epoxied to the ends. This allows a laser to pass unimpeded through the center of the hollow cathode. One of the two stainless steel flanges is connected to the inner coiled tubing to pass coolant into the vacuum cell. The cell is evacuated with a Welch pump (DuoSeal 1374, 10 L/s), and the cell pressure is monitored with a capacitance manometer.

C. Spectrometer

The plasma was probed by multipass direct absorption spectroscopy using a tunable difference frequency generation laser (DFG), which has been described previously.[27] The outputs of a 532 nm Nd:YVO_4 laser (Coherent Verdi V-10) and 622 nm tunable dye laser (Coherent 899-29, rhodamine

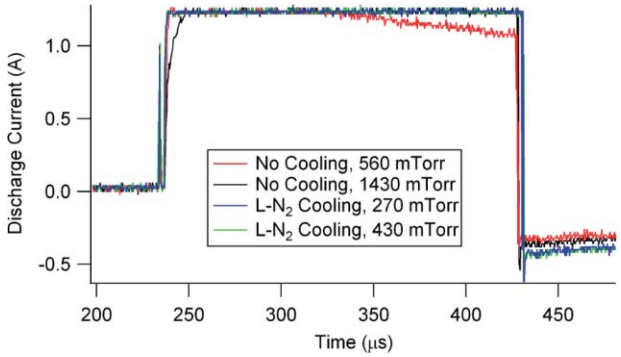

FIG. 2. Current during the discharge pulse for the four main sets of conditions used in this study. The discharge is started at $t \sim 230$ μs, and is cut off at $t \sim 430$ μs. Details about the choice of conditions are discussed in Secs. III B 1 and III C 1. The negative current after the discharge pulse is an artifact of the current monitor setup, which sees the pulser box recharging.

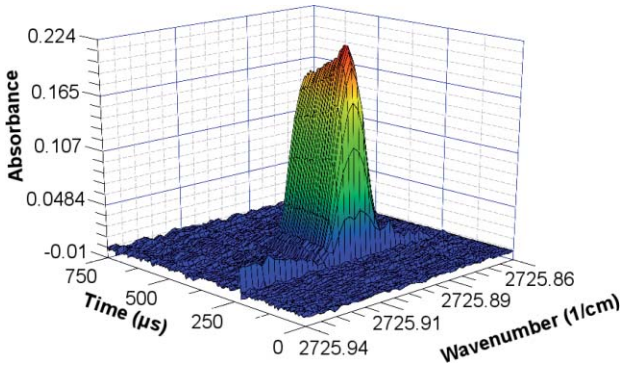

FIG. 3. A sample scan of the $R(1,0)$ transition of H_3^+ in a n-H_2 plasma produced by a liquid-nitrogen-cooled hollow cathode. The plot has been slightly modified for clarity by eliminating artifacts at the beginning and end of the discharge pulse resulting from electrical pickup.

640 dye) are combined in a MgO-doped periodically poled $LiNbO_3$ crystal, producing ~500 μW of tunable radiation around 2800 cm^{-1}. The DFG light was sent through the hollow cathode in a White-type multipass configuration, collected with a dc InSb detector, and the resultant signal stored on a computer for analysis. The InSb signal was ratioed with the signal from a silicon photodiode monitoring the dye laser to remove pump laser amplitude noise.

D. Analysis procedure

When a discharge pulse occurred, the InSb detector signal was recorded and split into two 750 μs intervals: a signal interval centered around the pulse, and a pretrigger interval for recording the background laser intensity. The latter interval was averaged over time, and the former binned and averaged into 150 5 μs intervals. Each of these was used to calculate a time-dependent absorbance signal: $-\ln(I/I_0)$, where I is the average laser intensity in the bin, and I_0 is the averaged background laser intensity. The binned absorbances were averaged over ten consecutive discharge pulses, and the laser was then stepped by ~0.002 cm^{-1}. This process was repeated until the absorption line was fully scanned, yielding a three-dimensional data set representing the spectrum as a function of time during the discharge pulse. Each transition was recorded three times for each set of conditions. A sample scan over a single transition is shown in Fig. 3.

The spectrum at each point in time for each individual scan is then fit to a Gaussian function to determine the integrated intensity and linewidth as a function of time. For each transition, the integrated intensity and inferred kinetic temperature (as determined from the measured linewidth) over time are averaged over the three scans, and the standard deviation of each quantity used as an estimate of the uncertainty. The plasma kinetic temperature is inferred from the average of all scans, and the rotational temperature is inferred from the relative intensities of the $R(1,1)^u$ and $R(2,1)^u$ transitions (the reasons for this are explained in Sec. III A).

As will be seen in Sec. IV, it is most convenient to express the *ortho*:*para* ratio of H_3^+ in terms of the fraction of p-H_3^+ (p_3). To calculate this quantity from the experimental data, we use the inferred rotational temperature to calculate

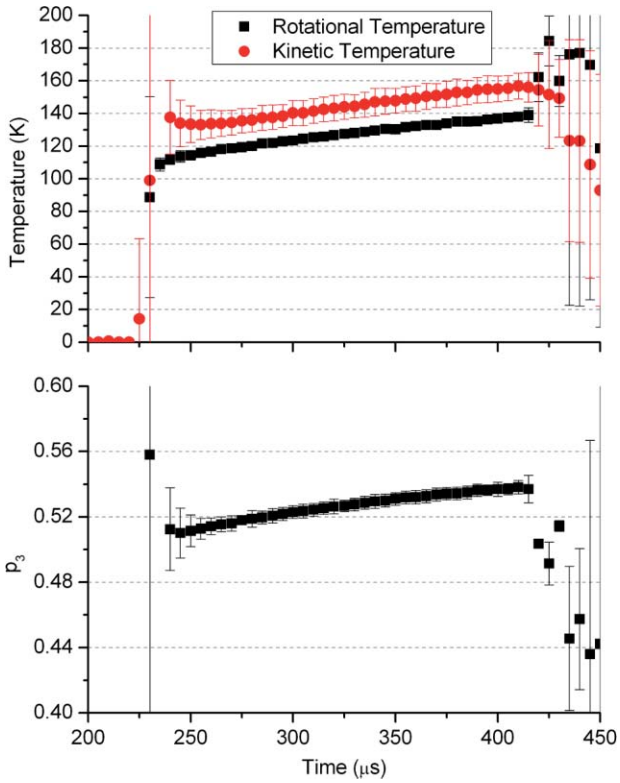

FIG. 4. Kinetic and rotational temperatures and p-H_3^+ fraction (p_3) inferred from measurements of the $R(1,0)$, $R(1,1)^u$, $R(2,2)^l$, and $R(2,1)^u$ transitions of H_3^+ in a liquid-nitrogen-cooled hollow cathode plasma consisting of 50% p-H_2. The discharge is started at $t \sim 220$ μs and is cut off at $t \sim 410$ μs.

separate Boltzmann distributions for the first 15 rotational levels of o-H_3^+ and p-H_3^+, using the forbidden (0,0) level energy as a common reference energy. The o-H_3^+ distribution is scaled to the population of the (1,0) level inferred from the $R(1,0)$ transition intensity, and likewise for p-H_3^+ with the (1,1) level population. For each subsequent level that was spectroscopically measured, the calculated population is replaced by the experimentally determined population. Finally, p_3 is calculated by dividing the sum of all *para* level populations by the sum of all level populations. An example of the results of the final calculation is shown in Fig. 4.

III. EXPERIMENTAL RESULTS

In this section, the results of a series of experimental measurements aimed at determining the value of α as a function of temperature are presented. First, we show measurements pertaining to the rotational thermalization of H_3^+ in the hollow cathode plasma. We then present parallel sections detailing measurements when the cell is uncooled, and when it is cooled with liquid nitrogen. Within each of these sections, measurements of the pressure dependence of the plasma chemistry and measurements of p_3 as a function of the p-H_2 fraction (p_2) at two different pressures are shown.

A. Thermalization measurements

To assess the degree of thermalization of the rotational levels of H_3^+ formed in the plasma and to validate the

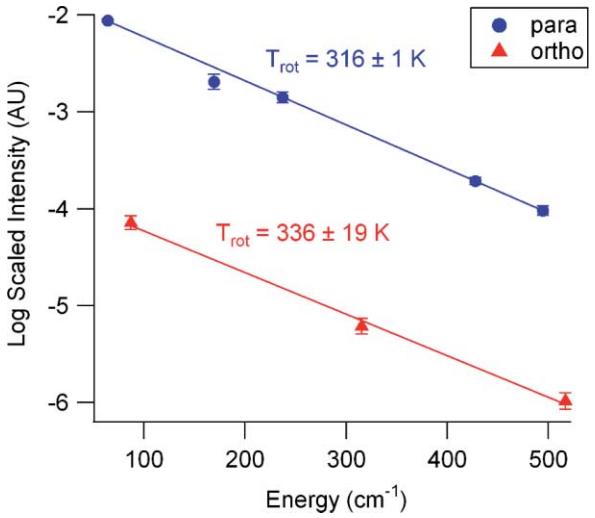

FIG. 5. Boltzmann plot of the first eight transitions of H_3^+ formed in a p-H_2 plasma. The data are taken at $t = 300$ μs, about 70 μs after the start of the discharge pulse. Because of systematic underpopulation, the population of the (2,2) level is not taken into account for the rotational temperature calculation of p-H_3^+.

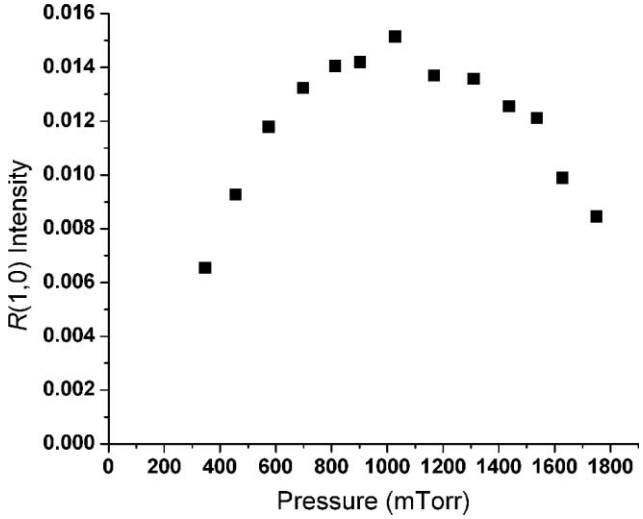

FIG. 6. R(1,0) inegrated intensity as a function of cell pressure in an uncooled n-H_2 plasma. The plotted data are selected at $t = 300$ μs. No error bars are shown, as only one scan was performed at each pressure.

calculation of p_3, all eight transitions listed in Table I were recorded in an uncooled p-H_2 plasma. A time slice of the data at 300 μs was taken and was subjected to a Boltzmann analysis, shown in Fig. 5. The kinetic temperature for this data set was found to be 319 ± 33 K, in good agreement with the inferred rotational temperatures for *ortho* (336 ± 19 K) and *para* (316 ± 1 K) H_3^+. A time slice taken at $t = 370$ μs gives similar results with slightly elevated temperatures: a kinetic temperature of 337 ± 29 K, o-H_3^+ rotational temperature of 339 ± 24 K, and p-H_3^+ temperature of 327 ± 1 K.

A noticeable feature in the plot is the underpopulation of the (2,2) level relative to all other *para* levels; this is a feature common to all data sets discussed in this work. Also, the o-H_3^+ rotational level distribution is thermal and consistent with the p-H_3^+ rotational temperature. Under liquid nitrogen conditions, only the $R(1,0)$ and $R(3,3)^l$ transitions of o-H_3^+ can be observed, and the signal-to-noise ratio of the $R(3,3)^l$ transition is low. Nevertheless, the o-H_3^+ rotational temperature, as inferred from the relative populations of the (1,0) and (3,3) levels, is consistent with the p-H_3^+ temperature. For these reasons, the relative populations of the (2,1) and (1,1) levels are used to calculate the rotational temperature of both o-H_3^+ and p-H_3^+ in the remainder of the data sets.

B. Uncooled measurements

1. Pressure dependence

As the goal of this work is to measure the hop:exchange ratio α in the reaction of H_3^+ with H_2, it is important to evaluate to what extent three-body collisions ($H_3^+ + 2H_2$) may influence the experimental measurements. As a first-order assessment, the intensity of the $R(1,0)$ transition was recorded as a function of cell pressure in a n-H_2 plasma. Because p_3, and temperature do not change greatly with changing pressure in a n-H_2 plasma (see Sec. III B 2), this measurement serves as a proxy for the H_3^+ number density in the cell.

The measurements are shown in Fig. 6. The $R(1,0)$ transition intensity initially increases with pressure, owing to the decreasing electron mobility (and therefore increasing charge density) with increasing cell pressure at constant electric current. However, at ~1000 mTorr, the trend begins to reverse, and the transition intensity decreases. Because the electron mobility should decrease monotonically with increasing pressure, the total ion density (equal to the electron density) must still be increasing, and therefore H_3^+ must be consumed by a chemical process leading to the formation of another stable ion. While not absolutely conclusive, it is likely that the reaction $H_3^+ + 2H_2 \rightarrow H_5^+ + H_2$ is responsible,[32,33] and this indicates that three-body effects may be present at some pressures.

In light of the pressure dependence observed in Fig. 6, measurements to determine the value of α are taken at two pressures. The lower pressure (560 mTorr) is chosen to be on the rising edge of the pressure curve, where it is likely that H_3^+ is the dominant ionic species in the plasma. The higher pressure (1430 mTorr) is chosen on the falling edge, where it is suspected that three-body collisions are occurring. A comparison of these data will assist in estimating the influence of three-body effects on the determination of α.

2. p-H_3^+ fraction

The $R(1,1)^u$, $R(1,0)$, $R(2,2)^l$, and $R(2,1)^u$ transitions of H_3^+ were recorded to determine the value of p_3 in plasmas with known p_2. For n-H_2 ($p_2 = 0.25$), the hydrogen gas was used continuously from the hydrogen generator, and for $p_2 = 0.999$, gas was used continuously from the p-H_2 converter. All other mixtures were prepared in advance. Measurements at both pressures (560 mTorr and 1430 mTorr) were performed in succession on the same day with the same gas mixture.

The observed transition intensities, inferred temperatures and p_3 values are presented in Table II, and p_3 is plotted as a function of p_2 in Fig. 7. Differences between the inferred

TABLE II. Integrated intensities of transitions from the lowest four rotational levels of H_3^+ in uncooled plasmas of varying p_2, with inferred kinetic and rotational temperatures and p_3 values. Numbers in parentheses represent 1σ uncertanties in the final digit(s).

Pressure (mTorr)	p_2	$R(1,1)^u$ cm^{-1}	$R(1,0)$ cm^{-1}	$R(2,2)^l$ cm^{-1}	$R(2,1)^u$ cm^{-1}	T_{kin} (K)	T_{rot} (K)	p_3
560	0.25	$4.92(46) \times 10^{-3}$	$1.52(4) \times 10^{-2}$	$5.11(21) \times 10^{-3}$	$4.79(24) \times 10^{-3}$	354(45)	367(57)	0.483(7)
	0.40	$7.87(65) \times 10^{-3}$	$1.73(8) \times 10^{-2}$	$5.69(39) \times 10^{-3}$	$6.11(47) \times 10^{-3}$	362(44)	275(34)	0.548(8)
	0.50	$4.73(16) \times 10^{-3}$	$9.22(35) \times 10^{-3}$	$5.86(28) \times 10^{-3}$	$4.45(3) \times 10^{-3}$	343(14)	349(17)	0.605(4)
	0.66	$9.79(40) \times 10^{-3}$	$1.30(7) \times 10^{-2}$	$8.52(28) \times 10^{-3}$	$7.44(71) \times 10^{-3}$	359(25)	269(30)	0.676(7)
	0.83	$6.46(18) \times 10^{-3}$	$5.41(41) \times 10^{-3}$	$6.18(13) \times 10^{-3}$	$5.67(7) \times 10^{-3}$	358(25)	318(12)	0.772(1)
	0.999	$9.93(20) \times 10^{-3}$	$4.58(27) \times 10^{-3}$	$7.73(18) \times 10^{-3}$	$7.91(32) \times 10^{-3}$	359(27)	283(15)	0.855(2)
1430	0.25	$5.18(55) \times 10^{-3}$	$1.47(5) \times 10^{-2}$	$5.13(46) \times 10^{-3}$	$4.11(16) \times 10^{-3}$	346(33)	282(36)	0.501(7)
	0.40	$7.08(48) \times 10^{-3}$	$1.51(13) \times 10^{-2}$	$6.17(28) \times 10^{-3}$	$5.70(39) \times 10^{-3}$	343(36)	287(32)	0.564(4)
	0.50	$5.97(3) \times 10^{-3}$	$1.04(6) \times 10^{-2}$	$6.46(8) \times 10^{-3}$	$5.17(29) \times 10^{-3}$	336(12)	313(22)	0.626(2)
	0.66	$8.18(87) \times 10^{-3}$	$1.13(5) \times 10^{-2}$	$6.79(68) \times 10^{-3}$	$6.55(68) \times 10^{-3}$	339(20)	285(48)	0.665(14)
	0.83	$7.87(10) \times 10^{-3}$	$6.57(7) \times 10^{-3}$	$8.21(18) \times 10^{-3}$	$7.06(5) \times 10^{-3}$	332(22)	327(7)	0.775(2)
	0.999	$1.01(3) \times 10^{-2}$	$4.41(30) \times 10^{-3}$	$8.58(53) \times 10^{-3}$	$8.22(43) \times 10^{-3}$	329(26)	290(20)	0.863(3)

values of p_3 between the two pressures are minor. The cell pressure does not seem to affect the p_3 vs p_2 distribution to any significant degree despite the pressure dependence seen in Fig. 6.

The inferred temperatures are plotted in Fig. 8. As mentioned in Sec. II D, the rotational temperatures reported in Table II are derived from the relative intensities of the $R(1,1)^u$ and $R(2,1)^u$ transitions. The quantity $T(2,2)$ in the plots is the inferred rotational temperature inferred from the $R(1,1)^u$ and $R(2,2)^l$ transitions, and it is consistently lower than the kinetic and rotational temperatures. This is due to the underpopulation of the (2,2) level alluded to in Fig. 5. The variance weighted means of T_{kin}, T_{rot}, and $T(2,2)$ are (351 ± 10) K, (310 ± 8) K, and (187 ± 5) K respectively for the low pressure data, and (336 ± 8) K, (320 ± 6) K, and (259 ± 5) K for the data set at 1430 mTorr.

C. Liquid-nitrogen-cooled "low temperature" measurements

1. Pressure dependence

The same experiment described in Sec. III B 1 for the uncooled plasma was carried out in a liquid-nitrogen-cooled n-H_2 plasma. The results are qualitatively similar to the high-temperature data, albeit shifted toward lower pressures, and are plotted in Fig. 9. The kinetic temperature was determined to be (128 ± 11) K for this data set. For the same purposes described earlier, a lower pressure of 270 mTorr and a higher pressure of 430 mTorr were chosen for the p_3 vs p_2 measurements.

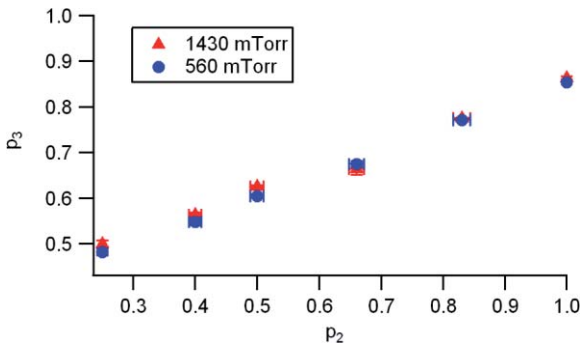

FIG. 7. Experimental measurements of p-H_3^+ fraction plotted against p-H_2 fraction for an uncooled plasma at 560 and 1430 mTorr.

2. p-H_3^+ fraction

Experiments analogous to those described in Sec. III B 2 were performed in a liquid-nitrogen-cooled hollow cathode.

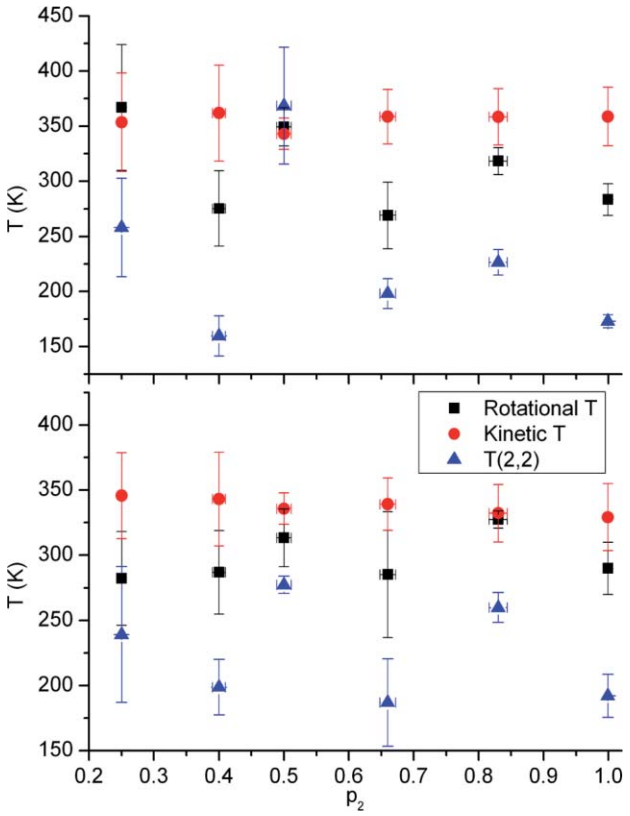

FIG. 8. Kinetic and rotational temperatures as a function of p-H_2 fraction in an uncooled plasma. Also plotted is the rotational temperature derived from comparison of the (2,2) and (1,1) levels, as an illustration of the underpopulation of the (2,2) level. Top: 560 mTorr. Bottom: 1430 mTorr.

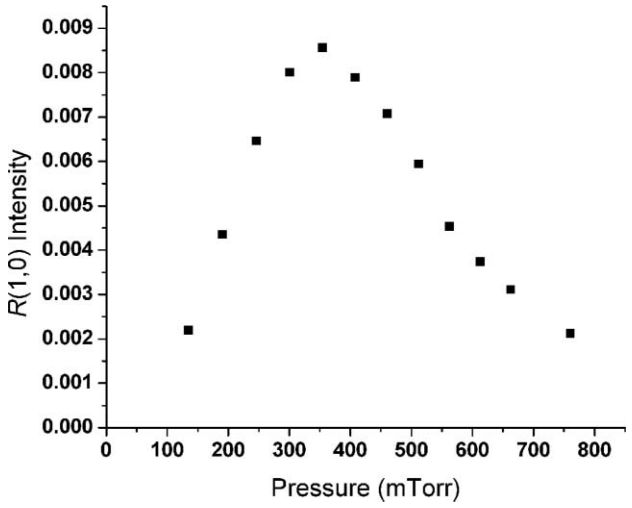

FIG. 9. $R(1,0)$ inegrated intensity as a function of cell pressure in a liquid-nitrogen-cooled n-H_2 plasma. The plotted data are selected at $t = 300\ \mu$s.

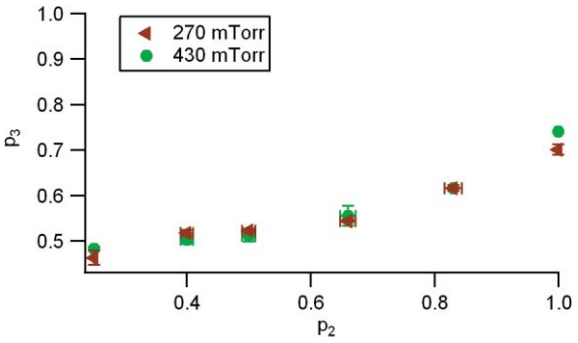

FIG. 10. Experimental measurements of p-H_3^+ fraction plotted against p-H_2 fraction for a liquid nitrogen cooled plasma at 270 and 430 mTorr.

The results are summarized in Table III, and plotted in Fig. 10. At the lower temperature, there is a noticeable difference between the 270 and 430 mTorr data sets. In particular, the data point at $p_2 = 0.999$ is significantly higher than the corresponding point at low pressure, although the remainder of the data points are quite similar. The inferred temperatures are plotted in Fig. 11. While T_{kin} remains constant with increasing p_2, T_{rot} and $T(2,2)$ markedly decrease, with the latter generally being lower. The variance-weighted mean of the kinetic temperature is (139 ± 4) K for the 270 mTorr data set, and (136 ± 5) K for the 430 mTorr set.

IV. ANALYSIS AND DISCUSSION

A. Steady state modeling

In order to extract the value of α from the experimental data, we have constructed steady state models that calculate p_3 as a function of p_2 and α. The full details of these models are presented in the previous article in this issue,[21] and the results are briefly summarized here.

The key assumption in these models is that the *ortho*:*para* ratio of H_3^+ in the hollow cathode plasma is predominantly determined by the reaction of H_3^+ with H_2. As a check of this assumption, we estimate the number of H_3^+-H_2 collisions that occur prior to destruction of H_3^+ by electron recombination (ambipolar diffusion is not a significant loss mechanism in a hydrogenic hollow cathode plasma[28]). In the uncooled n-H_2 plasma at 570 mTorr, we observe an H_3^+ ion density of $\sim 2 \times 10^{12}$ cm^{-3} with H_2 number density $\sim 1.5 \times 10^{16}$ cm^{-3}. Because H_3^+ is the dominant ion at this pressure, the electron density is also $\sim 2 \times 10^{12}$ cm^{-3}. The majority of these electrons are expected to be so-called "ultimate electrons," with a temperature on the order of 5000 K.[29,30] Using the H_3^+ electron recombination rate coefficient temperature scaling from storage ring measurements,[31] we estimate a dissociative recombination rate coefficient of $\sim 1 \times 10^{-8}$ cm^3 s^{-1}, and the rate coefficient for the $H_3^+ + H_2$ reaction is assumed to be the Langevin rate of $\sim 2 \times 10^{-9}$ cm^3 s^{-1}. Using these rate coefficients and densities, a single H_3^+ ion is expected to experience around 750 collisions with H_2 prior to its destruction by electron dissociative recombination. As steady state is expected to be reached in fewer than ten collisions,[21] this assumption should be valid.

For the uncooled plasma, we make a further assumption that the outcomes of the hop and exchange reactions are determined entirely by nuclear spin branching fractions.[16] This assumption is valid so long as sufficient energy is available

TABLE III. Integrated intensities of transitions from the lowest four rotational levels of H_3^+ in liquid-nitrogen cooled plasmas of varying p_2, with inferred kinetic and rotational temperatures and p_3 values. Numbers in parentheses represent 1σ uncertainties in the final digit(s).

Pressure (mTorr)	p_2	$R(1,1)^u$ cm^{-1}	$R(1,0)$ cm^{-1}	$R(2,2)^l$ cm^{-1}	$R(2,1)^u$ cm^{-1}	T_{kin} (K)	T_{rot} (K)	p_3
270	0.25	$9.11(82) \times 10^{-3}$	$2.71(9) \times 10^{-2}$	$5.81(15) \times 10^{-3}$	$2.82(15) \times 10^{-3}$	136(15)	136(8)	0.464(16)
	0.40	$1.38(4) \times 10^{-2}$	$3.16(5) \times 10^{-2}$	$7.36(12) \times 10^{-3}$	$3.48(12) \times 10^{-3}$	140(6)	123(3)	0.518(6)
	0.50	$1.52(5) \times 10^{-2}$	$3.27(11) \times 10^{-2}$	$7.04(28) \times 10^{-3}$	$3.86(7) \times 10^{-3}$	140(8)	123(2)	0.523(4)
	0.66	$1.42(5) \times 10^{-2}$	$2.75(14) \times 10^{-2}$	$6.03(13) \times 10^{-3}$	$2.80(8) \times 10^{-3}$	134(13)	110(2)	0.544(3)
	0.83	$1.82(5) \times 10^{-2}$	$2.43(5) \times 10^{-2}$	$5.39(26) \times 10^{-3}$	$3.23(20) \times 10^{-3}$	135(14)	105(3)	0.616(6)
	0.999	$2.02(9) \times 10^{-2}$	$1.83(2) \times 10^{-2}$	$5.77(56) \times 10^{-3}$	$2.88(10) \times 10^{-3}$	138(13)	96(2)	0.701(11)
430	0.25	$9.82(25) \times 10^{-3}$	$2.52(6) \times 10^{-2}$	$4.77(18) \times 10^{-3}$	$2.57(9) \times 10^{-3}$	136(10)	125(3)	0.483(4)
	0.40	$8.78(21) \times 10^{-3}$	$2.09(12) \times 10^{-2}$	$4.39(11) \times 10^{-3}$	$2.27(17) \times 10^{-3}$	138(10)	124(5)	0.503(9)
	0.50	$9.77(46) \times 10^{-3}$	$2.08(6) \times 10^{-2}$	$3.46(40) \times 10^{-3}$	$2.64(13) \times 10^{-3}$	141(16)	127(5)	0.512(13)
	0.66	$1.06(8) \times 10^{-2}$	$1.80(8) \times 10^{-2}$	$3.01(31) \times 10^{-3}$	$1.82(19) \times 10^{-3}$	132(22)	103(6)	0.556(22)
	0.83	$9.31(8) \times 10^{-3}$	$1.26(3) \times 10^{-2}$	$3.06(16) \times 10^{-3}$	$1.59(5) \times 10^{-3}$	129(14)	103(1)	0.617(1)
	0.999	$1.04(4) \times 10^{-2}$	$7.63(65) \times 10^{-3}$	$2.80(27) \times 10^{-3}$	$1.57(10) \times 10^{-3}$	137(13)	98(3)	0.741(1)

for many reactant and product states to be populated. The result, which we shall refer to as the "high temperature model," is

$$p_3 = \frac{\alpha + 2\alpha p_2 + 1}{3\alpha + 2}, \tag{4}$$

where p_3 is the p-H_3^+ fraction, p_2 is the p-H_2 fraction, and $\alpha \equiv k^H/k^E$ is the hop-to-exchange reaction rate ratio. This equation is a straight line that passes through $(p_3, p_2) = (0.5, 0.25)$ (n-H_3^+ and n-H_2, respectively) and whose slope is related to α.

Because of the pressure dependence discussed in Sec. III B 1, we have also constructed a high temperature model that includes the possibility of three-body spin-changing collisions of the form $H_3^+ + 2H_2 \rightarrow H_3^+ + 2H_2$. We assume that reactions leading to the formation of stable H_5^+ do not affect the p-H_3^+ fraction. In this case, p_3 is given by Eq. (5) (the "three-body high temperature model"), where α_2 is the same α from Eq. (4), α_3 is the three-body hop-to-exchange ratio, and Φ_2 is the branching fraction for reactive two body collisions compared to reactive three-body collisions:

$$p_3 = \frac{\frac{\Phi_2}{1+\alpha_2}\left(\frac{1}{3}\alpha_2 + \frac{2}{3}\alpha_2 p_2 + \frac{1}{3}\right) + \frac{1-\Phi_2}{1+\alpha_3}\left(\frac{39}{100}\alpha_3 + \frac{13}{50}\alpha_3 p_2 + \frac{19}{50} + \frac{3}{25}p_2\right)}{\frac{\Phi_2}{1+\alpha_2}\left(\alpha_2 + \frac{2}{3}\right) + \frac{1-\Phi_2}{1+\alpha_3}\left(\frac{91}{100}\alpha_3 + \frac{41}{50}\right)}, \tag{5}$$

$$p_3 = \frac{(k_{oopp} + k_{oopo})(1 - p_2) + k_{oppo}p_2}{(k_{oopp} + k_{oopo} + k_{poop} + k_{pooo})(1 - p_2) + (k_{oppo} + k_{ppoo})p_2}. \tag{6}$$

At the lower temperatures of the liquid-nitrogen-cooled plasma, energetic considerations may inhibit some reaction channels. For instance, conversion of p-H_2 to o-H_2 requires $E/k_B = 170$ K of energy, and so such processes might be expected to proceed more slowly in a colder plasma. In order to take this into account, a different derivation is employed, and Eq. (6) (the "low temperature model") results. In this equation, the rate coefficients k_{ijkl} represent the rates of reactions of the form i-$H_3^+ + j$-$H_2 \rightarrow k$-$H_3^+ + l$-H_2 (for instance, k_{oppo} is the rate coefficient for the reaction o-$H_3^+ + p$-$H_2 \rightarrow p$-$H_3^+ + o$-H_2). The rate coefficients are dependent on T_{kin}, T_{rot}, and the branching fractions for the identity, proton hop, and hydrogen exchange reactions (S^{id}, S^{hop}, and S^{exch}, where $\alpha \equiv S^{hop}/S^{exch}$), and they are calculated using a microcanonical statistical model.[20] Inclusion of three-body effects into this model is unfeasible owing to large numbers of unknown rate coefficients.

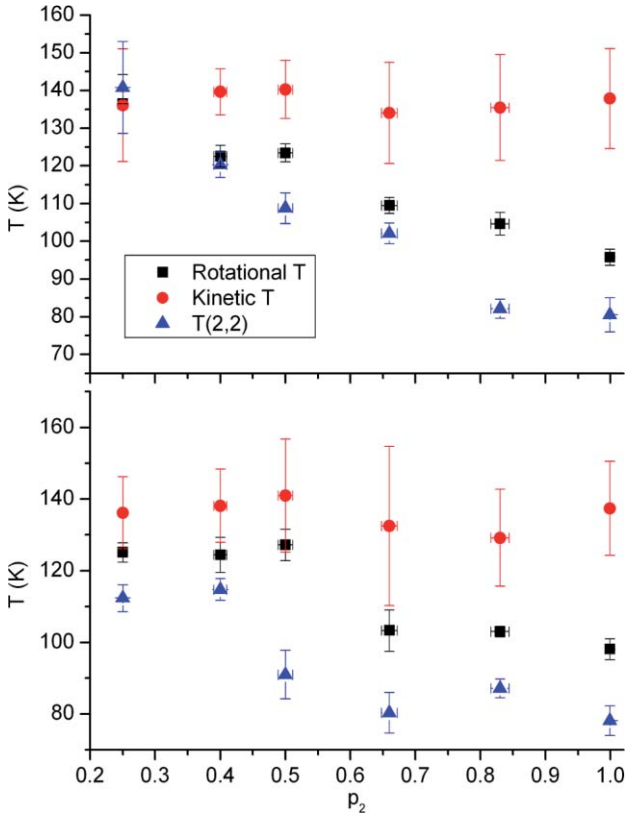

FIG. 11. Inferred temperatures as a function of p-H_2 fraction in a liquid nitrogen cooled plasma. Top: 270 mTorr. Bottom: 430 mTorr.

B. Uncooled plasma

By comparing the results of the high pressure and low pressure measurements in the context of Eqs. (4) and (5), the extent to which three-body collisions affect the determination of α can be assessed. The three-body high temperature model (Eq. (5)) reveals that for a given α_2, any three-body effects will cause the slope of a plot of p_3 vs p_2 to become more shal-

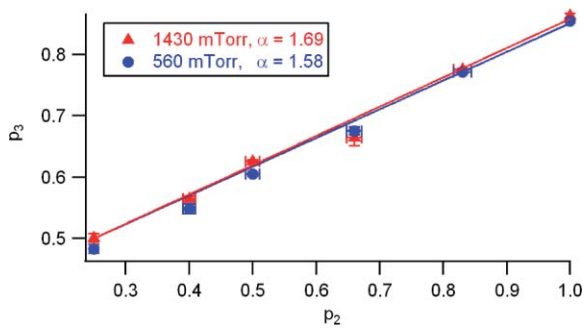

FIG. 12. High temperature model fits to experimental measurements in an uncooled plasma.

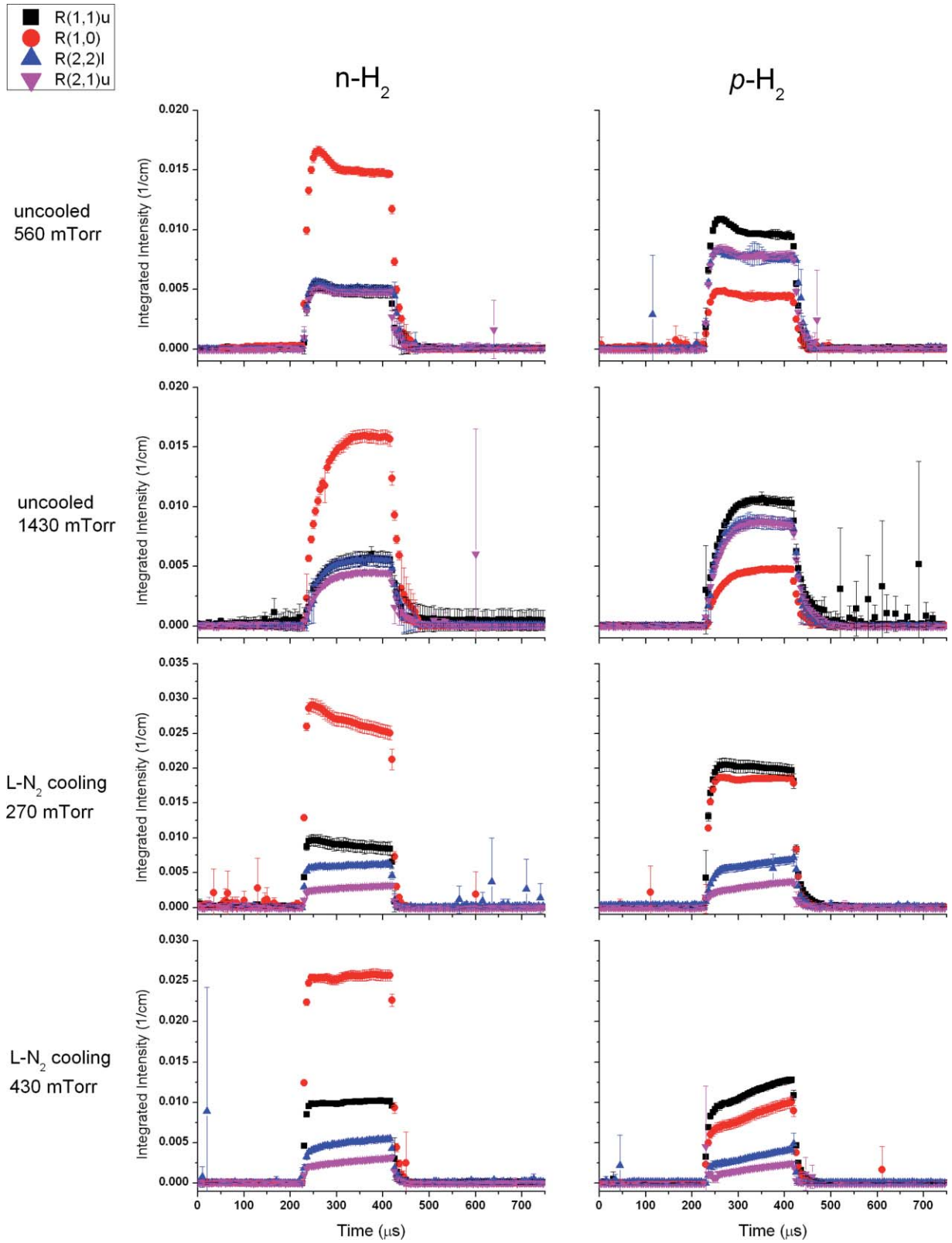

FIG. 13. Time dependence of inegrated intensities of all four observed transitions in n-H_2 ($p_2 = 0.25$, left) and p-H_2 ($p_2 = 0.999$, right) plasmas under the different temperature and pressure conditions explored in this work. The integrated intensities are averaged over three scans of each transition. Nonzero intensities outside of the pulse are the result of a blind Gaussian fit to a noise feature within a spectrum with no absorption, resulting in a spurious "inegrated intensity."

low (see Fig. 2 from previous article[21]). Therefore, if three-body effects are important, then a fit to the high temperature model (Eq. (4)) will underestimate α.

The term Φ_2 in the three-body high temperature model becomes smaller as the H_2 number density increases. If three-body proton-scrambling processes are important, a p_3 vs p_2 plot should give a shallower slope for measurements taken at a higher cell pressure (at the same temperature) compared to a lower pressure. As can be seen in Fig. 7, this was not observed in our data sets. We conclude that while there is evidence for H_5^+ formation in the cell, and therefore three-body collisions, these processes do not exhibit significant nuclear spin dependence under our experimental conditions, and therefore do not influence the value of α inferred from measurements in our uncooled plasma.

The data from the uncooled plasma are plotted in Fig. 12 along with fits to the high temperature model. The high pressure data fit reasonably well to the model, but the low pressure data are consistently below the model fit, especially at low p_2. This discrepancy is not due to three-body effects, but appears similar to curves produced by the low temperature model (Eq. (6)). It is possible that even at a temperature of $\sim$ 350 K, energetic effects may still restrict some of the possible reaction channels. Another possibility is that significant variation in state-to-state reaction cross sections causes the use of nuclear spin statistical weights to be inaccurate. Nevertheless, the data set at 560 mTorr gives $\alpha = 1.58$, and the set at 1430 mTorr gives $\alpha = 1.69$. We regard these as being within the overall experimental uncertainty, although the uncertainty in the fits are only 0.02 and 0.03, respectively.

Cordonnier *et al.*[17] performed a similar measurement in a pulsed hollow cathode plasma. They measured the ratio of the transition intensities of the $R(1,0)$ and $R(1,1)^u$ transitions in n-H_2 and p-H_2 plasmas at a pressure of 1.85 Torr and temperature of $\sim$ 400 K. Using a detailed chemical model of their plasma together with their measurements ($p_3 = 0.893$ at $p_2 = 0.999$), they derived $\alpha = 2.4$, with an uncertainty of at least 0.6. As validation, inserting their results into Eq. (4) gives $\alpha = 2.46$.

An issue discussed in their work is the back-conversion of p-H_2 to o-H_2 in their plasma over the course of a discharge pulse. This is illustrated in their Fig. 2. For comparison, our results are plotted in a similar format in Fig. 13. The time dependence of our signals most closely resembles theirs for the 1430 mTorr data set. Note the relatively slow rise of H_3^+ absorption, and the slight increase in the $R(1,0)$ inegrated intensity over time in the p-H_2 measurement at 1430 mTorr. This effect is not observed in the 560 mTorr data set. We suspect that the higher ion density in the 1430 mTorr data set results in more H atom recombination on the walls of the cathode, which forms H_2 in the "normal" 3:1 *ortho*:*para* ratio in quantities large enough to significantly affect the overall p-H_2 fraction. The higher pressure and discharge current (2.8 A) reported by Cordonnier *et al.* likely caused more back-conversion in their experiment than in ours. For our calculation of α, we have chosen data points early on in the discharge pulse when these effects are minimal.

Our derived values for α around 1.6 fall just below the lower limit of the estimated uncertainty of the results of Cordonnier *et al.* Our temperature of $\sim$ 350 K is lower than theirs, and a decrease of α with temperature is in line with expectations from statistical arguments. The value of α inferred from measurements of the $D_3^+ + H_2$ isotopic system by Gerlich[11] is $\sim$ 1.6 at a collision energy of $\sim$ 44 meV, which corresponds roughly to a temperature $T = (2/3)(E/k_B) = 340$ K, in excellent agreement with our results.

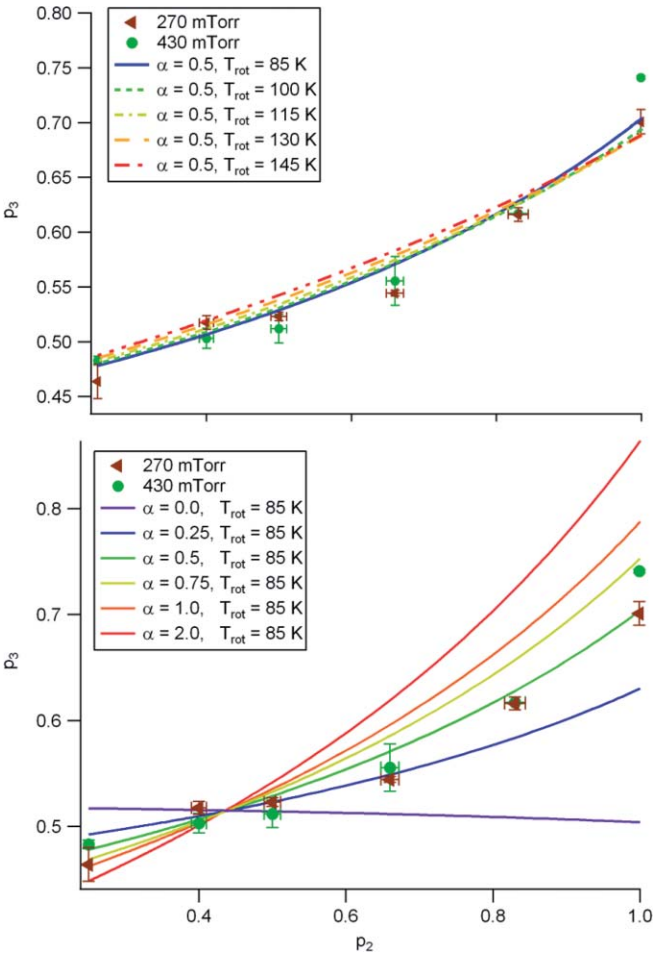

FIG. 14. Comparison of the data from the liquid nitrogen cooled hollow cathode with calculations from the low temperature model (Eq. (6)). For all curves shown, $T_{kin} = 135$ K and $S^{id} = 0.1$.

C. Liquid-nitrogen-cooled plasma

Unlike the case of high temperature, with our current models we are unable to make predictions about the change in a plot of p_3 vs p_2 with pressure (hence, three-body interactions) at low temperature. It has been observed that the rates of ternary association reactions leading to the formation of H_{2n+1}^+ clusters increase with decreasing temperature.[32,33] However, it is unclear whether this process is dependent on the nuclear spin configuration of H_3^+. It is, however, dependent on the nuclear spin of H_2; the rate coefficient for ternary association of H_3^+ with p-H_2 at 10 K is over an order of magnitude faster than with n-H_2.[33] This may account for the differences in the time traces in the lowest pair of plots in Fig. 13.

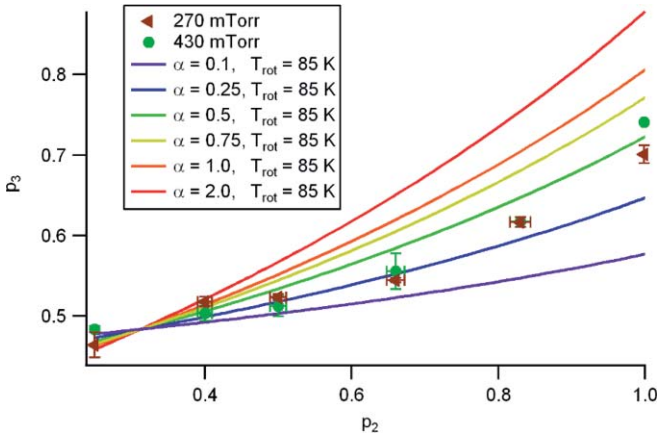

FIG. 15. Comparison of the data from the liquid nitrogen cooled hollow cathode with calculations from the low temperature model (Eq. (6)). For all curves shown, $T_{kin} = 135$ K and $S^{id} = 0.9$.

At both pressures, the temperatures plotted in Fig. 11 suggest that higher energy levels of p-H_3^+ are being selectively destroyed at a faster rate as the p-H_2 fraction increases. Although the (3,3) level of o-H_3^+ was not observed during these measurements, our thermalization measurements (see Sec. III A) suggest that the behavior of o-H_3^+ is the same as p-H_3^+. Also, the time traces within individual conditions in Fig. 13 do not display significantly different time dependence between o-H_3^+ and p-H_3^+, after considering the increasing temperature and possibly a small amount of p-H_2-to-o-H_2 back-conversion.

To model the p_3 vs p_2 curves, rate coefficients k_{ijkl} were calculated with $S^{id} = 0.1$ (the statistical value), $\alpha = \{0, 0.1, 0.5, 2, 10, \infty\}$, T_{kin}=135 K, and T_{rot}={85−145} K in steps of 15 K. Several of these curves are plotted along with the experimental results for comparison in Fig. 14. For the data set at 270 mTorr, the data agree well with rate coefficients calculated with $\alpha = 0.5$, no matter the rotational temperature used. Because the apparent rotational temperature decreases with increasing p_2, the most appropriate comparison would involve multiple low temperature model curves, but these only differ by a small amount. A more important effect is the change of the shape in the p_3 vs p_2 curve as a function of α (Fig. 14, lower panel).

The higher pressure data do not fit as well with the calculated curves. This might be due to a greater influence of nuclear-spin-dependent three-body processes not taken into account by our model. As mentioned before, H_5^+ formation has been observed to be faster in a p-H_2 plasma, and this may have some effect on the p-H_3^+ fraction at high pressure and high p-H_2 fraction. Because of the uncertainties here, we do not attempt to express a value of α for the 430 mTorr data set. We conclude that in our 139 ± 4 K plasma, the value of α is 0.5 ± 0.1. This suggests that even at this relatively modest temperature, the $(H_5^+)^*$ collision complex has a lifetime sufficient to allow for full scrambling.

Recently, Crabtree *et al.* have used a modified version of the low-temperature model to study the *ortho*:*para* ratio of H_3^+ in diffuse molecular clouds.[9] While their usage of the model includes some parameters related to interstellar chemistry, they found that their best match to astronomical observations required the value of S^{id} to be large, on the order of 0.9. To see if this value is consistent with our data, we have calculated rate coefficients for $S^{id} = 0.9$, $T_{kin} = 135$ K, $T_{rot} = 85$ K, and a range of α values. The results are plotted in Fig. 15. Each of the curves is shifted upwards slightly at higher p_2 relative to the corresponding curve in Fig. 14 (lower), but the curve at $\alpha = 0.5$ still agrees with the data reasonably well. It is possible that a lower value of α would provide a more optimal agreement, but this difference is likely within our total experimental uncertainty. It is not surprising that changing the value of S^{id} by such a large amount has a relatively small influence on the calculated p_3 values. This is because all of the rate coefficients in the low temperature model are reactive rate coefficients (i.e., none of them involve

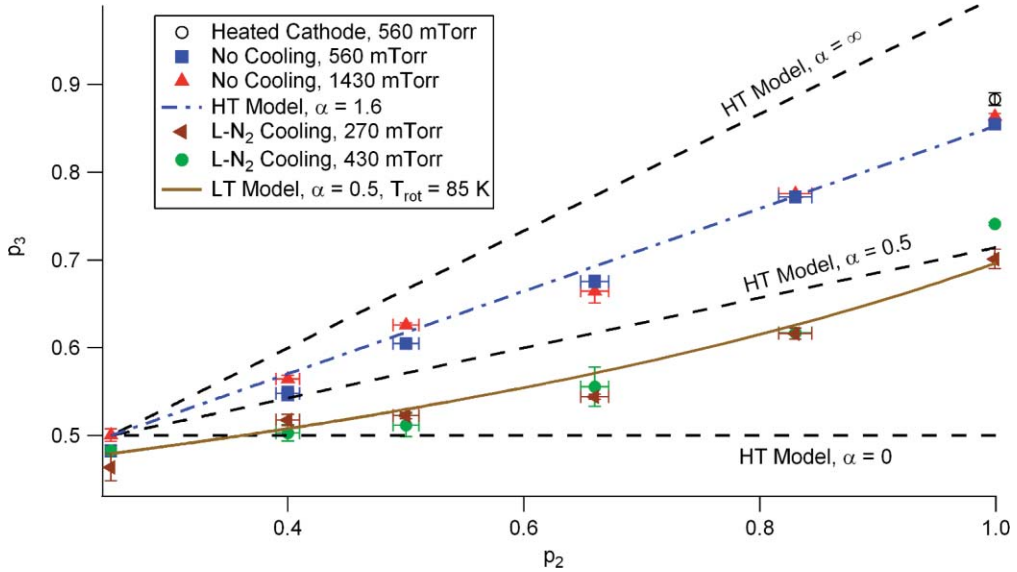

FIG. 16. Summary of all experimental data and the best estimates for α for each temperature. Also shown for reference are high temperature model traces for $\alpha = \{0, 0.5, \infty\}$.

the identity pathway). The effect of increasing S^{id} is essentially just to scale all of the rate coefficients down by a roughly constant factor.

Comparison of the liquid nitrogen cooled data with the uncooled data indicate that, as observed in the $D_3^+ + H_2$ system,[11] α decreases with temperature, as illustrated in Fig. 16. Even without the use of models, the decrease in α is evident by looking at the p-H_3^+ fraction formed in a plasma of pure p-H_2. In such a plasma, the H_3^+ produced by the $H_2^+ + H_2$ reaction is entirely p-H_3^+, and the formation of o-H_3^+ proceeds only through the $H_3^+ + H_2$ reaction. The nuclear spin selection rules for $H_3^+ + H_2$ show that for p-$H_3^+ + p$-H_2, the only way for o-H_3^+ to be formed is via the exchange process. Therefore, the decrease in p_3 at $p_2 \sim 1$ from high temperature to low temperature suggests that the exchange reaction becomes more dominant.

To further confirm this trend, we used a fluid circulator to pass heated ethylene glycol at 100 °C through the cathode. We then performed measurements of the $R(1,0)$, $R(1,1)^u$, $R(2,2)^l$, and $R(2,1)^u$ transitions in a 99.9% p-H_2 plasma at 560 mTorr. The kinetic temperature obtained was 450 ± 75 K, and the inferred p_3 value was 0.883 ± 0.007, corresponding to $\alpha = 2.2 \pm 0.3$. While this measurement is only at one value of p_2, the p_3 value is significantly higher than the corresponding value in the 350 K plasma, which is consistent with a higher hop:exchange ratio at higher temperature.

V. CONCLUSIONS

We have studied the nuclear spin dependence of the reaction of H_3^+ with H_2 by monitoring the populations of the four lowest rotational levels of H_3^+ formed in plasmas of varying p-H_2 enrichment. For the first time, this reaction has been studied at low temperature by cooling a hollow cathode discharge cell, resulting in a plasma temperature of 135 K. Using steady-state chemical models, the ratio of the rates of the proton hop and hydrogen exchange reactions (α) has been inferred at two different temperatures: 1.6 ± 0.1 at 350 K, and 0.5 ± 0.1 at 135 K. These values can be compared favorably with previous studies of this reaction at ~400 K ($\alpha = 2.4 \pm 0.6$),[17] preliminary measurements at 450 K ($\alpha = 2.2 \pm 0.3$), and measurements of the analogous $D_3^+ + H_2$ system.[11]

In spite of the good agreement between the experimental data and steady state models, some of the results hint at a greater level of complexity than treated here. The (2,2) level of p-H_3^+ is consistently underpopulated relative to the kinetic temperature of the gas in our plasmas, and the rotational temperature of H_3^+ decreases with increasing p-H_2 fraction in our liquid nitrogen cooled cell. It is unclear whether the origin of these effects is ternary association reactions to form H_5^+, or state-to-state processes not accounted for in our models.

To remove any ambiguity in these results, it will be necessary to perform similar measurements in the carefully-controlled conditions of an ion trap. In such an environment, the gas density can be kept low enough to preclude three-body processes, and the temperature can be lowered beyond the 135 K achieved in this work. Fully quantum reactive scattering calculations on the H_5^+ potential energy surface, combined with our results and ion trap measurements, would help greatly in furthering our understanding of this fundamental process.

ACKNOWLEDGMENTS

The authors would like to thank Takayoshi Amano for providing designs and helpful suggestions for the hollow cathode cell used in this work. We thank Kisam Park for providing a computer program for calculating the rate coefficients used in our low temperature model. This work was supported by NSF PHY 08-55633.

[1] P. G. Jambrina, F. J. Aoiz, C. J. Eyles, V. J. Herrero, and V. S. Rabanos, J. Chem. Phys. **130**, 184303 (2009).
[2] C. W. Eaker and G. C. Schatz, J. Phys. Chem. **89**, 2612 (1985).
[3] J. E. Pollard, L. K. Johnson, D. A. Lichtin, and R. B. Cohen, J. Chem. Phys. **95**, 4877 (1991).
[4] W. D. Watson, Astrophys. J. **183**, L17 (1973).
[5] E. Herbst and W. Klemperer, Astrophys. J. **185**, 505 (1973).
[6] B. J. McCall, T. R. Geballe, K. H. Hinkle, and T. Oka, Astrophys. J. **522**, 338 (1999).
[7] B. J. McCall, K. H. Hinkle, T. R. Geballe, G. H. Moriarty-Schieven, N. J. Evans, II, K. Kawaguchi, S. Takano, V. V. Smith, and T. Oka, Astrophys. J. **567**, 391 (2002).
[8] N. Indriolo, T. R. Geballe, T. Oka, and B. J. McCall, Astrophys. J. **671**, 1736 (2007).
[9] K. N. Crabtree, N. Indriolo, H. Kreckel, B. A. Tom, and B. J. McCall, Astrophys. J. **729**, 15 (2011).
[10] T. J. Millar, A. Bennett, and E. Herbst, Astrophys. J. **340**, 906 (1989).
[11] D. Gerlich, J. Chem. Soc., Faraday Trans. **89**, 2199 (1993).
[12] D. Gerlich, E. Herbst, and E. Roueff, Plan. Space Sci. **50**, 1275 (2002).
[13] D. Gerlich, F. Windisch, P. Hlavenka, R. Plail, and J. Glosik, Phil. Trans. R. Soc. London, Ser. A **364**, 3007 (2006).
[14] E. Hugo, O. Asvany, and S. Schlemmer, J. Chem. Phys. **130**, 164302 (2009).
[15] M. Quack, Mol. Phys. **34**, 477 (1977).
[16] T. Oka, J. Mol. Spectrosc. **228**, 635 (2004).
[17] M. Cordonnier, D. Uy, R. M. Dickson, K. E. Kerr, Y. Zhang, and T. Oka, J. Chem. Phys. **113**, 3181 (2000).
[18] Z. Xie, B. J. Braams, and J. M. Bowman, J. Chem. Phys. **122**, 224307 (2005).
[19] A. Aguado, P. Barragán, R. Prosmiti, G. Delgado-Barrio, P. Villarreal, and O. Roncero, J. Chem. Phys. **133**, 024306 (2010).
[20] K. Park and J. C. Light, J. Chem. Phys. **126**, 044305 (2007).
[21] K. N. Crabtree, B. A. Tom, and B. J. McCall, J. Chem. Phys., **134**, 194310 (2011).
[22] C. M. Lindsay and B. J. McCall, J. Mol. Spectrosc. **210**, 60 (2001).
[23] L. Neale, S. Miller, and J. Tennyson, Astrophys. J. **464**, 516 (1996).
[24] B. A. Tom, S. Bhasker, Y. Miyamoto, T. Momose, and B. J. McCall, Rev. Sci. Instrum. **80**, 016108 (2009).
[25] T. Amano, J. Opt. Soc. Am. B **2**, 790 (1985).
[26] See supplementary material document at http://dx.doi.org/10.1063/1.3587246 for detailed schematics of the hollow cathode discharge cell.
[27] K. N. Crabtree, C. A. Kauffman, and B. J. McCall, Rev. Sci. Instrum. **81**, 086103 (2010).
[28] T. Amano, J. Chem. Phys. **92**, 6492 (1990).
[29] J. S. Dobrosavljević and D. S. Pešić, Appl. Spectrosc. **35**, 57 (1981).
[30] P. A. Büger and W. Fink, Z. Phys. **236**, 314 (1970).
[31] B. J. McCall, A. J. Huneycutt, R. J. Saykally, N. Djuric, G. H. Dunn, J. Semaniak, O. Novotny, A. Al-Khalili, A. Ehlerding, F. Hellberg, S. Kalhori, A. Neau, R. D. Thomas, A. Paal, F. Öhsterdahl, and M. Larsson, Phys. Rev. A. **70**, 052716 (2004).
[32] R. Johnsen, C.-M. Huang, and M. A. Biondi, J. Chem. Phys. **65**, 1539 (1976).
[33] W. Paul, B. Lücke, S. Schlemmer, and D. Gerlich, Int. J. Mass Spec. Ion Proc. **149–150**, 373 (1995).